

Spectra of infrared reflection and Raman scattering of light of crystals with a belousovite structure from first principles

© Yu.N. Zhuravlev

Kemerovo State University, Kemerovo, Russia

e-mail: zhur@kemsu.ru

Received July 03, 2024

Revised August 26, 2024

Accepted August 27, 2024

In the full-electron and pseudopotential basis of localized atomic orbitals with the exchange-correlation functional PBE and the dispersion correction D3 of the CRYSTAL code, the crystal structure, dielectric constant tensor, LO-TO mode splitting, infrared reflection spectra and Raman scattering of the mineral belousovite and its synthetic analogues with formula $AZnSO_4X$ ($A = K, Rb, Cs, Tl$; $X = Cl, Br, I$). The presence of SO_4 , ZnO_3X tetrahedra and AO_nX_m polyhedra in the structure is shown, which appear in different regions of the vibrational spectra. In polarized reflection spectra, SO_4 modes have high-intensity bands ν_1 and ν_3 from 900 to 1160 cm^{-1} , formed by vibrations of nonequivalent oxygen atoms. In the lattice region below 150 cm^{-1} , vibrations involving cation atoms are distinguished. Individual modes with a high level of LO-TO splitting have been identified. In the Raman spectrum, the most intense modes will also be ν_1, ν_3 . The first group consists of four modes, where the most intense one at $900\text{--}920\text{ cm}^{-1}$ is formed largely by vibrations of individual nonequivalent oxygen atoms, and the other three by sulfur atoms and other atoms. On the contrary, modes with wavenumbers above 1100 cm^{-1} have an overwhelming contribution from O4 oxygen atoms with the shortest S-O and A-O distances. For these and other modes, linear dependences of wave numbers on interatomic distances, average atomic masses and radii of cations A and anions X have been established.

Keywords: belousovite, synthetic crystals, *ab initio*, dielectric constant, infrared reflectance spectra, Raman spectra.

DOI: 10.61011/EOS.2024.08.60035.6851-24

Introduction

Natural mineral belousovite was discovered in Tolbachik volcano (the Kamchatka Peninsula) [1]. It occurs in the form of irregular-shaped grains and microcrystalline masses associated with other minerals. About 350 mineral species have been identified in the Tolbachik fumaroles, including 123 minerals first discovered here.

Species diversity and specifics of this mineralization are attributable to unique combination of physical and chemical conditions and mineralization mechanisms: high temperatures, atmospheric pressure, ultrahigh oxygen fugacity, gas-phase transfer of most chemical elements and direct deposition of many high-temperature minerals from volcanic gases with a specific geochemical composition [2].

Empirical formula of belousovite is $K_{0.97}Rb_{0.01}Zn_{1.00}S_{1.01}O_{4.03}C_{10.97}$, and the ideal formula is $KZnSO_4Cl$. This is a monoclinic crystal with space group $P2_1/c$ whose structure is studied in detail in [1]. As reported in [3], the belousovite crystal structure is actually an archetype for a large family of isostructural synthetic compounds $AZnTO_4X$ ($A = K, Rb, Cs, Tl, NH_4$; $T = S, Se$; $X = Cl, Br, I$) that form a morphotropic series and were obtained by melting and evaporation through reaction between AX and $ZnTO_4$ either at high temperatures or in hot water solutions. From them, only

two synthetic compounds $RbZnSO_4Cl$ and $TlZnSO_4Cl$ have been described previously [4].

As long as the $AZnSO_4X$ structures have been obtained relatively recently, experimental studies of their physical properties are not available. In this view, *ab initio* computer simulation methods are essential. Such approach ensures practical predictability of microstructures and macroproperties of functional crystalline materials, because it determines microscopic atomic and electronic properties of materials and provides uniform description of their macroscopic properties. It is also able to acquire a large amount of data on material properties and simulate effectively extreme conditions that are difficult to achieve experimentally. Finally, such approach makes it possible to design materials and properties desired by researchers to provide the opportunities for future experimental search [5,6]. *Ab initio* methods are widely used to examine vibrational spectra of crystals [7–9].

Vibrational spectroscopy (infrared (IR) reflection and Raman scattering (RS)) is a powerful tool for identification of sulfate minerals [10], detail investigation of structure and chemical bonding of alkaline and alkaline-earth metals using experimental [11–14] and theoretical [15] methods. Spectra are usually described on an assumption that vibrations are divided into internal — stretching and deformation vibrations for $[SO_4]$ and external — translational vibrations for cations, anions, and librational vibrations for sulfate

groups. Theoretical group analysis gives distribution of free anion vibrations by irreducible representations of the point symmetry group T_d and vibration activity in the IR and RS spectra:

$$\Gamma_{\text{vib}} = A_1(\text{KPC}) + E(\text{KPC}) + 2F_2(\text{OR, RS}),$$

that correspond to the intramolecular modes $\nu_1, \nu_2, \nu_3, \nu_4$. For the breathing mode $\nu_1(A_1)$ of the free $[\text{SO}_4]^{2-}$ ion, the frequency is equal to [16] $971\text{--}993\text{ cm}^{-1}$, for the triply-degenerate stretching mode $\nu_3(F_2)$ — the frequency is equal to $1070\text{--}1190\text{ cm}^{-1}$. Deformation vibrations have lower frequencies: doubly-degenerate $\nu_2(E)$ — $445\text{--}490\text{ cm}^{-1}$, and triply-degenerate $\nu_4(F_2)$ — $613\text{--}648\text{ cm}^{-1}$. Four IR absorption features were identified at ~ 1105 , ~ 983 , ~ 611 and $\sim 450\text{ cm}^{-1}$ in sulfate anion in water [17], which corresponds to asymmetric stretching ν_3 , symmetric stretching ν_1 , asymmetric bending ν_4 and symmetric bending ν_2 , respectively.

In the spectra of crystals containing sulfate anions, vibration frequencies are shifted depending on the nature of cations, electronegativity, weight, ionic radius and crystal structure. Crystal structure defines the symmetry of $[\text{SO}_4]$ groups, number of formula units in lattice, possible splitting of degenerate modes and resonance vibration interaction, which increases the number of bands in spectra and causes significant difficulties in interpretation.

Thus, structural features are important aspects in formation of vibrational properties of disulfate halides, and computer-assisted methods serve as a convenient tool for investigation. Therefore, the objective of this study is to identify a correlation between structural features and vibrational properties of crystalline sulfates with belousovite structure AZnSO_4X ($A = \text{K, Rb, Cs, Tl}$; $X = \text{Cl, Br, I}$).

Calculation method

Vibrational properties of the studied crystals were investigated by density functional theory (DFT) methods in combination with the Hartree-Fock approximation using CRYSTAL software package [18]. Crystal orbitals are defined by linear combinations of the Gaussian type localized atomic orbitals, the exponents and coefficients of which are determined from an all-electron set for oxygen atoms [19], sulfur atoms [20], zinc atoms [21] and chlorine atoms [22]. Pseudopotential basis sets [23] were used for bromine and iodine atoms, and double and triple zeta valence polarized sets (DZVP and TZVP) [24,25]. DFT generalized gradient approximation used an exchange-correlation functional of one of the most common PBE forms [26] supplemented by the empirical dispersion correction in form of D3(BJ) [27]. The PBE+D3 functional gives good resultant structural parameters, but is inferior to hybrid functional in the accuracy of vibrational spectra calculation [28]. The accuracy control thresholds for the Coulomb and exchange series are set to 8, 8, 8, 8, 16 [29]. The reciprocal space is discretized using the Monkhorst-Pack grid [30] with 30

independent \mathbf{k} -points in the irreducible part of the Brillouin zone. Accuracy of the self-coupling procedure was not lower than 10^{-9} a.u. (1 a.u. = 27.21 eV).

Crystalline structures were optimized using analytical energy gradients both by lattice cell parameters and atom coordinates within the quasi-Newton scheme in combination with the Broyden–Fletcher–Goldfarb–Shanno (BFGS) algorithm [31–34]. convergence was checked both by the gradient components and nuclear shift for which default values were chosen [29].

Vibration frequencies were derived by diagonalization of the dynamic matrix calculated by numerical differentiation of the analytical full energy gradient with respect to Cartesian coordinates of atoms. For details of the harmonic vibration calculation, see [35,36]. Optimized equilibrium geometry was used.

Transverse optical (TO) vibration frequencies $\nu_{\text{TO},n}$ in point Γ ($\mathbf{k} = 0$, center of the first Brillouin zone) are derived from diagonalization of the mass-weighted Hessian matrix.

$$W_{\alpha i, \beta j} = \frac{H_{\alpha i, \beta j}}{\sqrt{M_\alpha M_\beta}}.$$

Here, $H_{\alpha i, \beta j}$ is the second derivative of energy calculated numerically from analytical gradients, M_α and M_β are atomic weights; Greek and Latin indices correspond to atoms and Cartesian coordinates, respectively. longitudinal optical (LO) frequencies $\nu_{\text{LO},n}$ may be calculated taking into account that the dynamic matrix in ionic and semi-ionic compounds is written as a sum of two summands:

$$W_{\alpha i, \beta j} = W_{\alpha i, \beta j} + W_{\alpha i, \beta j}^{\text{NA}}(\mathbf{k} \rightarrow 0).$$

Nonanalytic correction [37] to the dynamic matrix occurs due to the parallel polarization and phonon wave vector. LO frequencies are then calculated by diagonalization of the full (i.e. analytic + nonanalytic) dynamic matrix. From knowing them, TO–LO-splitting can be calculated. TO and LO frequencies are calculated as maxima $\varepsilon_2(\nu)$ and minima ($-1/\varepsilon_2(\nu)$) (loss functions) of the imaginary part of the complex permittivity $\varepsilon(\nu) = \varepsilon_1(\nu) + i\varepsilon_2(\nu)$.

Oscillator strengths

$$f_{n,ij} = \frac{1}{4\pi\varepsilon_0} \frac{4\pi}{V} \frac{Z_{n,i}Z_{n,j}}{\nu_{\text{TO},n}^2}$$

were calculated for each TO mode using the Born vector

$$Z_{n,i} = \sum_{\alpha} t_{n,\alpha j} Z_{\alpha,ij}^* \frac{1}{\sqrt{M_\alpha}} \quad [38].$$

Here, ε_0 is the vacuum permittivity, V is the lattice cell volume, $t_{n,\alpha i}$ is the element of the Hessian eigen vector matrix W , $Z_{\alpha,ij}^*$ are the effective atomic Born tensors calculated using the Berry phased approach [39].

The permittivity tensor $\varepsilon(\nu)$ is calculated for each non-equivalent polarization direction according to the classical Drude–Lorentz model:

$$\varepsilon(\nu) = \varepsilon_{\infty,ii} + \varepsilon_{0,ii} = \varepsilon_{\infty,ii} + \sum_n \frac{(f_{n,ii} \nu_{\text{TO},n}^2)}{\nu_{\text{TO},n}^2 - \nu^2 - i\nu\gamma_n},$$

where ii denotes the polarization direction; $\varepsilon(\infty)$ is the static permittivity tensor at $\lambda \rightarrow \infty$; ν_n, f_n and n are the TO frequency, oscillator strength and decay coefficient for the n th vibrational mode, respectively. The reflectance curve $R(\nu)$ is calculated for each nonequivalent polarization direction using the following equation

$$R_{ii}(\nu) = \left| \frac{\sqrt{\varepsilon_{ii}(\nu) - \sin^2 \theta} - \cos \theta}{\sqrt{\varepsilon_{ii}(\nu) - \sin^2 \theta} + \cos \theta} \right|^2,$$

where θ is the angle between the incident beam and normal to the crystal surface [40].

Electronic components of the static permittivity tensor are related to the corresponding polarizability components α as follows:

$$\varepsilon_{\infty,ij} = \delta_{ij} + \frac{\alpha_{ij}}{\varepsilon_0 V},$$

where δ_{ij} is the Kronecker delta symbol and the polarizability is calculated using the coupled Hartree-Fock perturbation method (CPHF) [41]. The electronic components virtually don't depend on the IR range frequency because the electronic transition energies are very high compared with the vibrational energies. The permittivity tensor is a symmetric second-rank tensor. If it is diagonalized, then square roots of eigenvalues $n_i = \sqrt{\varepsilon_i}$ ($i = 1, 2, 3$) will correspond to the main refractive indices of the medium. Ionic contributions to the permittivity ε_0 are introduced as a sum of oscillator strengths [42].

Relative Raman peak intensities are calculated analytically by using a scheme that is an extension of the IR absorption intensity calculation [43].

Crystal structure

Correctness of the *ab initio* calculation of the $AZnSO_4X$ ($A = K, Rb, Cs, Tl; X = Cl, Br, I$) crystal structure was assessed using the rms deviation Δ of theoretical data from experimental data [3] by 27 structural parameters, including lattice constants a, b, c , monoclinic angle β , volume V , four distances R_{A-O}, R_{S-O} , three distances R_{Zn-O} , one R_{A-X} and R_{Zn-X} each, and nine angles O-A-O, O-Zn-X, O-S-O. The maximum deviation was max. 2.9%, which is a satisfactory result for such complex compounds. Substantial contribution to Δ is made by distances S-O in sulfate ion that differ for four nonequivalent oxygen atoms O1-O4. As long as these are exactly the distances that are essential for intramolecular vibrations, were included them in Table 1 for all belousovite type crystals.

Crystal structures of belousovite and its synthetic analogs (hereinafter referred to as AZSX) contain one symmetrically independent $[SO_4]$ group. tetrahedra are distorted, the minimum distance was found for S-O4, the maximum distance was found for S-O2 in sulfate chlorides (hereinafter referred to as AZSC): $KZnSO_4Cl$ (hereinafter referred to as KZSC), $RbZnSO_4Cl$ (hereinafter referred to as RZSC), $CsZnSO_4Cl$ (hereinafter referred to as CZSC), $TlZnSO_4Cl$

(hereinafter referred to as TZSC); S-O3 in sulfate bromides (hereinafter referred to as AZSB): $KZnSO_4Br$ (hereinafter referred to as KZSB), $RbZnSO_4Br$ (hereinafter referred to as RZSB), $CsZnSO_4Br$ (hereinafter referred to as CZSB), $TlZnSO_4Br$ (hereinafter referred to as TZSB) and in sulfate iodides AZSI: $RbZnSO_4I$ (hereinafter referred to as RZSI), $CsZnSO_4I$ (hereinafter referred to as CZSI). Zn atoms have the tetrahedral coordination ZnO_3X , where the shortest distances will be Zn-O1 (KZSC, RZSC), Zn-O2 (CZSC, TZSC), Zn-O3 in AZSB, AZSI. Zn-X distances increase with the ionic radius of halide X (Cl, Br, I). Polyhedra of metal atoms A (K, Rb, Cs, Tl) have the environments AO_5X_3 in KZSC, AO_6X_3 in KZSB, RZSC, RZSB, CZSB, TZSB, AO_7X_3 in CZSC, TZSC and unique RbO_6I_2 , CsO_7 in iodides. In all AZSX, the shortest distance falls on A-O4 and increases in series X as the cation's ionic radius grows. The following distances will be A-O3 (KZSC, KZSB, RZSC, RZSB, RZSI, TZSB), A-O1 (CZSC, TZSC), A-O2 (CZSB, CZSI). A-X in the halide series grows with the cation's ionic radius. Taking into account the coordination environment of cations A and halides X their mean ionic radius R_{AX} [44] grows in the chloride, bromide and iodide series. Thus, some structural parameters may be written as a linear dependence, for example

$$V(\text{\AA}^3) = 342.9 + 53.4R_{AX}^3.$$

Dielectric properties

Optical response of a material is described by its dielectric function $\varepsilon_{ij}(\nu)$ [45]. For a monoclinic system, it is a symmetric tensor that has non-zero components $\varepsilon_{xx}, \varepsilon_{yy}, \varepsilon_{zz}, \varepsilon_{xz} = \varepsilon_{zx}$ in the x, y and z reference axes. Element ε_{xz} is responsible for rotation of dielectric axes and is quite low for the electronic part ($|\varepsilon_{\infty,xz}| < 0.04$ in AZSC, CZSB, CZSI, TZSB and < 0.08 in the rest compounds) and is higher for the ionic part ($|\varepsilon_{0,xz}| < 0.1$ in KZSB, RZSI, CZSC, CZSI and > 0.1 in the rest compounds). Angle between the optical axes will be maximum in TZSB, where it is equal to 60.9° , in RZSC — 46.2° , TZSC — 36.3° . Its lowest values falls on KZSC — 5.0° and CZSI — 7.8° . As long as ε is a symmetric tensor, it may be written in a diagonal form with $\varepsilon_x, \varepsilon_y, \varepsilon_z$. Diagonal components of the dielectric electronic tensor ε_∞ and ionic tensor ε_0 are listed in Table 2.

Dielectric properties of the studied crystals have not been studied experimentally, therefore the data listed in Table 2 are predictive. Theoretical methods are widely used to predict dielectric properties of new materials [46]. Dielectric tensors of many crystals may be also found here. Calculation (experimental) data [40] or dielectric tensor components of the orthorhombic aragonite $CaCO_3$ are given or comparison: $\varepsilon_{\infty,xx} = 2.181$ (2.33), $\varepsilon_{\infty,yy} = 2.66$ (2.81), $\varepsilon_{\infty,zz} = 2.674$ (2.82), $\varepsilon_{0,xx} = 6.406$ (6.74), $\varepsilon_{0,yy} = 15.588$ (10.41), $\varepsilon_{0,zz} = 8.087$ (7.78). There is significant dielectric property anisotropy in crystals with belousovite structure as well as in the known aragonite.

Table 1. Lattice constants a, b, c , angle β and distance between the S and O atoms R_{S-O} (Å) in the $AZnSO_4X$ monoclinic crystals calculated using the PBE-D3 functional and measured experimentally [3] (Exp)

Crystal	Method	a , Å	b , Å	c , Å	β , grad	R_{S-O4}	R_{S-O1}	R_{S-O3}	R_{S-O2}
KZnSO ₄ Cl	Exp	6.9324	9.606	8.2227	96.524	1.430	1.479	1.479	1.480
	PBE-D3	6.9770	9.6655	8.2640	96.732	1.4712	1.5225	1.5272	1.5275
KZnSO ₄ Br	Exp	7.0420	9.7207	8.4233	98.201	1.435	1.484	1.487	1.483
	PBE-D3	7.0759	9.7524	8.4468	98.391	1.4699	1.5239	1.5321	1.5250
RbZnSO ₄ Cl	Exp	7.2692	9.6261	8.3178	95.524	1.4337	1.4826	1.4779	1.4858
	PBE-D3	7.3817	9.7368	8.3623	94.831	1.4724	1.5225	1.5249	1.5318
RbZnSO ₄ Br	Exp	7.3573	9.7091	8.5753	97.820	1.4330	1.4800	1.4852	1.4837
	PBE-D3	7.4831	9.7625	8.7012	98.079	1.4695	1.5234	1.5324	1.5275
RbZnSO ₄ I	Exp	7.5036	9.8981	8.8015	99.175	1.433	1.487	1.492	1.482
	PBE-D3	7.5803	9.9704	8.8752	99.255	1.4684	1.5268	1.5367	1.5260
CsZnSO ₄ Cl	Exp	7.6854	9.6794	8.4492	95.303	1.431	1.478	1.476	1.477
	PBE-D3	7.8732	9.7065	8.2733	93.227	1.4753	1.5210	1.5217	1.5378
CsZnSO ₄ B	Exp	7.7892	9.7910	8.7355	97.290	1.430	1.478	1.480	1.482
	PBE-D3	7.8579	9.8412	8.8578	97.674	1.4708	1.5232	1.5314	1.5277
CsZnSO ₄ I	Exp	9.449	8.311	9.393	96.982	1.444	1.481	1.486	1.484
	PBE-D3	9.5371	8.3104	9.4411	97.640	1.4760	1.5220	1.5356	1.5231
TlZnSO ₄ Cl	Exp	7.341	9.622	8.1632	94.012	1.451	1.498	1.484	1.504
	PBE-D3	7.5034	9.5621	8.0490	92.910	1.4762	1.5192	1.5238	1.5374
TlZnSO ₄ Br	Exp	7.3746	9.7060	8.3810	96.370	1.434	1.480	1.475	1.480
	PBE-D3	7.5375	9.7782	8.6777	98.258	1.4707	1.5230	1.5331	1.5273

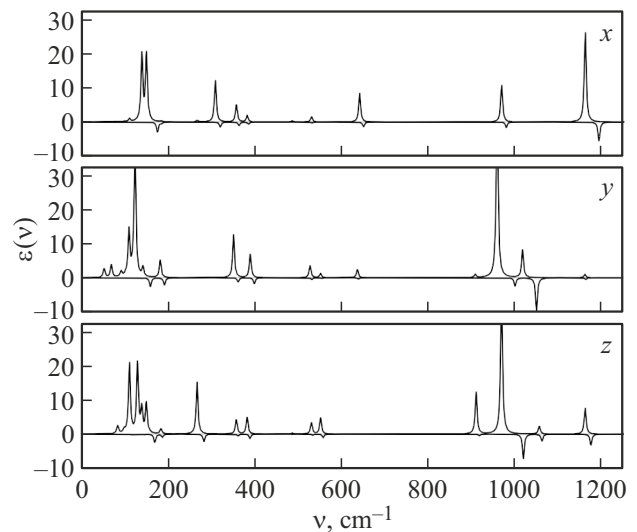
Table 2. Diagonal components of the electronic ϵ_∞ and ionic ϵ_0 dielectric tensors of belousovite type crystals.

Crystal	$\epsilon_{\infty,x}$	$\epsilon_{\infty,y}$	$\epsilon_{\infty,z}$	$\epsilon_{0,x}$	$\epsilon_{0,y}$	$\epsilon_{0,z}$
KZnSO ₄ Cl	2.36	2.26	2.26	2.08	3.53	3.95
KZnSO ₄ Br	2.50	2.31	2.29	2.05	3.60	3.81
RbZnSO ₄ Cl	2.19	2.11	2.12	2.08	3.25	3.77
RbZnSO ₄ Br	2.29	2.12	2.12	1.86	3.04	3.18
RbZnSO ₄ I	2.46	2.18	2.19	2.18	3.21	2.93
CsZnSO ₄ Cl	2.42	2.33	2.34	2.88	3.74	4.40
CsZnSO ₄ Br	2.48	2.31	2.30	1.86	3.04	3.18
CsZnSO ₄ I	2.63	2.22	2.22	2.64	3.26	6.96
TlZnSO ₄ Cl	2.97	2.82	2.81	4.08	4.69	8.14
TlZnSO ₄ Br	2.97	2.80	2.75	3.27	4.68	4.36

The permittivity tensor components ϵ_∞ are defined by the electronic subsystem of the crystal. This is indicated by the tensor dependences on subsystem parameters. For polycrystals, the mean value that, according to [46], is calculated as

$$\epsilon_{\infty,av} = (\epsilon_{\infty,x} + \epsilon_{\infty,y} + \epsilon_{\infty,z})/3,$$

depends linearly on the bond energy E_b calculated are the difference of the total lattice cell energy and the energy of constituent atoms $\epsilon_{\infty,av} = 9.97 + 0.04\Delta E_b(0.86)$ or dispersion energy component $\epsilon_{\infty,av} = -0.27 - 0.54E_{disp}(0.89)$. Here, the energies are measured in electronvolts, and expansion coefficients are set such that to achieve a dimensionless permittivity. Correlation coefficients of such dependence are given in brackets. Similarly to [46], dependence

**Figure 1.** Frequency dependence of the x -, y -, z -components of the imaginary part of the dielectric tensor $\epsilon_2(\nu)$ (top) and loss function $-1/\epsilon_2(\nu)$ (bottom) in KZnSO₄Cl.

on the band gap was established with high correlation coefficient 0.93: $\epsilon_{\infty,av} = 3.57 - 0.57\Delta E_g$.

Figure 1 shows the frequency dependence of the dielectric tensor, its imaginary part $\epsilon_2(\nu)$ and loss function $-1/\epsilon_2(\nu)$ for x -, y - and z -components in KZSC. Maxima of $\epsilon_2(\nu)$ and minima of the loss function correspond to TO- and LO-frequencies, respectively.

In the sulfate ion vibration ν_3 region, two TO modes of symmetry B_u with the wave numbers of 1162, 1056 cm^{-1}

and two TO modes of symmetry A_u with 1164, 1020 cm^{-1} will be active and displayed in the $\varepsilon_2(\nu)$ spectra with different intensity. LO modes have only the A_u symmetry with their values for this region equal to 1165, 1052 cm^{-1} . Thus, TO–LO splitting is equal to -1.1 and -32.2 cm^{-1} . In the vibration range ν_1 , two active modes also have different TO–LO splitting. Thus, the LO mode 1002 cm^{-1} has splitting of 41.5 cm^{-1} , while the mode at 910 cm^{-1} has only 0.4 cm^{-1} . The degree of splitting depends on the interaction coefficient that can be characterized as overlapping between the LO and TO mode eigen vectors. Eigen vector for each mode consists of the quantitative x -, y -, z -shifts of each atom in the lattice cell. Thus, the eigen vectors of the mode with the wave number of 910 cm^{-1} have 99% overlapping with the TO mode 910 cm^{-1} and, therefore, corresponding splitting was so small. For the ν_4 type vibrations, the spectrum will have closely-spaced TO modes of symmetry B_u, A_u with the wave numbers of 641, 637 cm^{-1} and the LO mode at 640 cm^{-1} . For the ν_2 region, a series of low-intensity peaks is observed with the TO modes of symmetry B_u 551, 530, 485 cm^{-1} , and for A_u symmetry, 552 (TO–LO splitting is equal to -1.5 cm^{-1}), 528 (3.6), 487 (0.0) cm^{-1} are observed.

Table 3 shows the LO frequencies of intense vibrations ν_1 – ν_4 and the corresponding LO–TO splitting (in brackets) of the AZSX crystals. Wave numbers of the LO modes are generally higher than of TO, therefore, the TO–LO shift is negative. Positive values of $-(\text{TO} - \text{LO})$ are given in Table 3 for clarity. However, inversions occur in some cases. Thus, in RZSC, the LO mode with the wave number of 1005 cm^{-1} has eigen vector overlapping with the TO modes of 966 and 1016 cm^{-1} at 64 and 76%. All modes with larger TO–LO splitting exhibit overlapping equal to or lower than 75%. The reason is that this overlapping is associated with substantial diagonal (W) and off-diagonal (W^{NA}) contributions. Thus, in all ten AZSX crystals, one mode with the highest wave number ν_3 exhibits almost 100% overlapping of eigen vectors corresponding to the LO and TO modes. This circumstance is due to the fact that the eigen vectors of the corresponding LO and TO modes are generated by the prevailing contribution of the x -, z -shifts of the O4 atoms and much lower contribution of the S atoms.

IR reflection spectra

Infrared spectroscopy (IRS) is widely used in various fields of physics and chemistry to identify the structure of compounds, in particular, to determine whether functional groups and other fragments are present. As identified previously, $[\text{SO}_4]$, ZnO_3X , AO_nX and m fragments are displayed in the studied AZnSO_4X crystals. It is of interest to plot theoretical IR absorption spectra and to determine how these structural features are displayed in them. Such data will be predictive for future experimental studies.

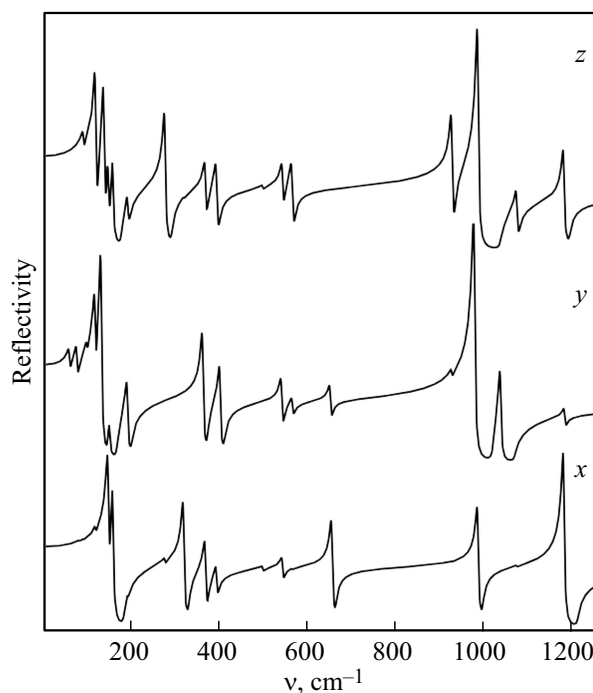


Figure 2. Reflection spectra of KZnSO_4Cl for polarizations $\mathbf{E} \parallel x$, $\mathbf{E} \parallel y$, $\mathbf{E} \parallel z$.

Theoretical IR reflection spectra were obtained by the Gaussian broadening of intensities of normal longwave ($\mathbf{k} = 0$) vibrations using the procedure described in [47].

Reflection spectra $R(\nu)$ are calculated from the dielectric function that is plotted on the basis of a set of damped oscillators (one per each normal mode) characterized by frequencies (wave numbers ν_j), oscillator strengths f_j and decay coefficients γ_j . Decay coefficients are not available from the initial calculations and shall be selected in accordance with the known experimental criteria. In case when such criteria are not available, then some value averaged over the literature data shall be selected. This simulation used $\gamma = 5 \text{ cm}^{-1}$ or all crystals. Figure 2 shows the IR reflection spectra of KZSC in the range from 0 to 1250 cm^{-1} .

Spectrum $R(\nu)$ for the x -, z -directions is defined by the TO modes of symmetry B_u . In both spectra, vibrations with the wave numbers of 1162, 969 cm^{-1} will be displayed, however, their intensity will be different. Moreover, for the ν_3, ν_1 region, there will be also vibrations with the wave numbers of 1056 and 910 cm^{-1} in the z -direction. On the contrary, the vibration ν_4 with the wave number of 641 cm^{-1} will be distinguished only in the x -polarization. Modes ν_4 will have the wave numbers of 551, 530, 485 cm^{-1} , two last numbers of which will be distinguished in both spectra. For the lattice region lower than 400 cm^{-1} , two vibrations 381, 356 cm^{-1} with intensities in the x - and z -polarizations and vibrations 266, 149 and 138 cm^{-1} may be distinguished. The last two vibrations have high intensity in the x -polarization. On the contrary, vibrations with the

Table 3. Wave numbers of the vibrational LO modes ($-(TO-LO)$ splitting) in the $AZnSO_4X$ crystals. All values are given in cm^{-1} .

Crystal	ν_3	ν_1	ν_4	ν_2
KZnSO ₄ Cl	1165(1.1), 1052(32.2)	1002(41.5), 910(0.4)	640(2.5)	552(1.5), 531(3.6)
KZnSO ₄ Br	1169(3.7), 1040(20.0)	996(48.1), 905(0.0)	631(1.5)	559(0.7), 538(5.2)
RbZnSO ₄ Cl	1163(0.1), 1005(-11.5)	1053(86.6), 910(0.4)	643(2.3)	546(2.4), 523(1.0)
RbZnSO ₄ Br	1173(3.0), 1035(16.8)	997(51.2), 904(0.0)	631(1.4)	558(0.7), 536(4.8)
RbZnSO ₄ I	1174(3.7), 1028(11.2)	988(51.5), 898(0.2)	622(0.7)	560(0.7), 537(4.6)
CsZnSO ₄ Cl	1148(1.7), 1000(-2.1)	1039(66.0), 905(0.3)	635(1.7)	545(3.2), 532(0.2)
CsZnSO ₄ Br	1162(1.7), 1035(17.0)	991(44.1), 907(0.0)	632(1.8)	555(0.7), 532(3.5)
CsZnSO ₄ I	1162(24.2), 1025(4.7)	970(18.9), 889(0.0)	609(8.9)	588(1.4), 547(0.2)
TlZnSO ₄ Cl	1128(0.8), 994(-0.0)	1024(60.7), 900(0.2)	628(1.5)	546(3.6), 533(0.3)
TlZnSO ₄ Br	1148(2.6), 1027(16.7)	979(39.2), 904(0.0)	628(1.8)	553(0.5), 529(3.8)

wave numbers of 128, 110 cm^{-1} will be shown only in the z -polarization.

Each vibrational mode is characterized by the polarization vector indicating the atomic displacement direction, and the normalized squared amplitude indicates their relative contribution to the total deviation. Thus, for example, the wave number of 110 cm^{-1} is corresponded by the atomic vibrations of zinc (9%), chlorine (14%), O1, O4 (22% each) and O2, O3 (15% each). Vibration at 128 cm^{-1} involves the potassium (12%), zinc (8%), chlorine (21%), sulfur (8%) and all oxygen atoms, except O3. For modes 138 and 149 cm^{-1} , the percentage of K atoms is about 37%, O2 and O3 atoms is 20% and O1, O4 atoms is 20% as well. In the former - zinc percentage (8%) is observed, in the latter — sulfur percentage (6%) is observed. In the mode with a wave number of 266 cm^{-1} , O4 (50%), O2 (19%) atoms prevail, zinc and sulfur (7% each) are also involved. Mode 308 cm^{-1} that is active only in the x -polarization is induced by the atomic vibrations of Zn (12%) and Cl (59%) with minor involvement of O1 and O3 atoms. Finally, modes 381 and 356 cm^{-1} are defined by the prevailing involvement of O atoms with a substantial contribution of O1 and O3 equal to 52% and 63%, respectively.

The y -polarized spectrum $R(\nu)$ is characterized by vibrations with symmetry A_u . A band at 961 cm^{-1} formed by the atomic vibrations of S (27%), O1 (30%) and O3 (41%) will be the most intense and taken equal to 100%. Bands with lower intensity of $\sim 38\%$ at 910 and 1020 cm^{-1} formed mainly by the atomic vibrations of O2, O3, O1 and O2, respectively, are on the left and right. Vibrations at 390, 351 cm^{-1} are induced by atomic displacement of mainly O1 and O3 with a Zn atom percentage (6%) observed for the latter. Lattice modes with high intensity at 123, 109 cm^{-1} are induced by the atomic vibrations of K (21%), Zn (7%) and O, where O2 contribution (30%) is distinguished.

For ease of comparison, Figure 3 shows reflection spectra normalized to unity for all ten $AZnSO_4X$ crystals. Wave numbers of intense lattice vibrations are listed in Table 4.

The obtained wave numbers of atomic vibrations in the $AZnSO_4X$ crystals are within the previous measurements for other sulfates. According to [17], the features of internal vibrations are displayed at $\sim 1050-1250$ (ν_3), ~ 1000 (ν_1),

Table 4. Wave numbers of intense TO modes with symmetries A_u ($-(TO-LO)$ splitting) and B_u in the lattice region of the $AZnSO_4X$ crystals. All values are given in cm^{-1} .

Crystal	A_u	B_u
KZnSO ₄ Cl	389(9.3), 351(10.5), 123(35.6)	308, 266, 149, 138
KZnSO ₄ Br	389(3.5), 349(15.9), 101(7.9)	351, 259, 152, 104
RbZnSO ₄ Cl	386(11.4), 341(8.8), 115(34.0)	309, 268, 131, 106
RbZnSO ₄ Br	386(1.9), 347(17.2), 112(17.8)	349, 260, 128, 104
RbZnSO ₄ I	385(0.3), 333(18.9), 146(11.1)	331, 254, 122, 106
CsZnSO ₄ Cl	390(6.7), 326(11.6), 108(-4.4)	335, 254, 131, 106
CsZnSO ₄ Br	380(1.9), 346(15.4), 112(9.8)	347, 260, 125, 91
CsZnSO ₄ I	326(12.5), 134(10.6)	330, 265, 196, 183
TlZnSO ₄ Cl	329(6.0), 307(9.1), 117(34.7)	338, 263, 130, 112
TlZnSO ₄ Br	381(2.5), 347(12.9), 105(5.7)	347, 266, 128, 95

$\sim 500-700$ (ν_4) and $\sim 400-500$ (ν_2) cm^{-1} . lattice vibrations, including metal-oxygen, librational and translational, are observed in the region $< 400\text{ cm}^{-1}$. Thus, in [48], the wave numbers of IR active vibrations of the $ZnSO_4$ water solution were measured: ν_3 — 1102, 1153, 1185 cm^{-1} , ν_1 — 997, 1010, 1020 cm^{-1} , ν_4 — 605, 624, 656, 667 cm^{-1} and for ν_2 - a very faint peak at 420 cm^{-1} . According to [16], in $SrSO_4$ for ν_3 , frequencies 1195, 1130, 1095 cm^{-1} were measured, ν_1 — 990 cm^{-1} and ν_4 — 639, 610 cm^{-1} , and in [17], a set of 1238, 1128, 991, 648, 614 cm^{-1} is also added by 471 cm^{-1} . IR spectra of $K_2Zn(SO_4)_2 \cdot 6H_2O$ and $Rb_2Zn(SO_4)_2 \cdot 6H_2O$ solid solutions with symmetry $P2_1/C$ were also measured [49] and support the previous behaviors. In the first and seconds cases for ν_3 (ν_1), 1141, 1108, 1102 cm^{-1} (982 cm^{-1}) and 1139, 1111, 1099 cm^{-1} (984 cm^{-1}) were recorded, respectively Thus, the vibration wave numbers calculated for the belousovite type crystals agree with the experimental measurements for alkali sulfates and zinc sulfate.

RS spectra

RS spectroscopy is an effective method for chemical analysis and examining the composition and structure of

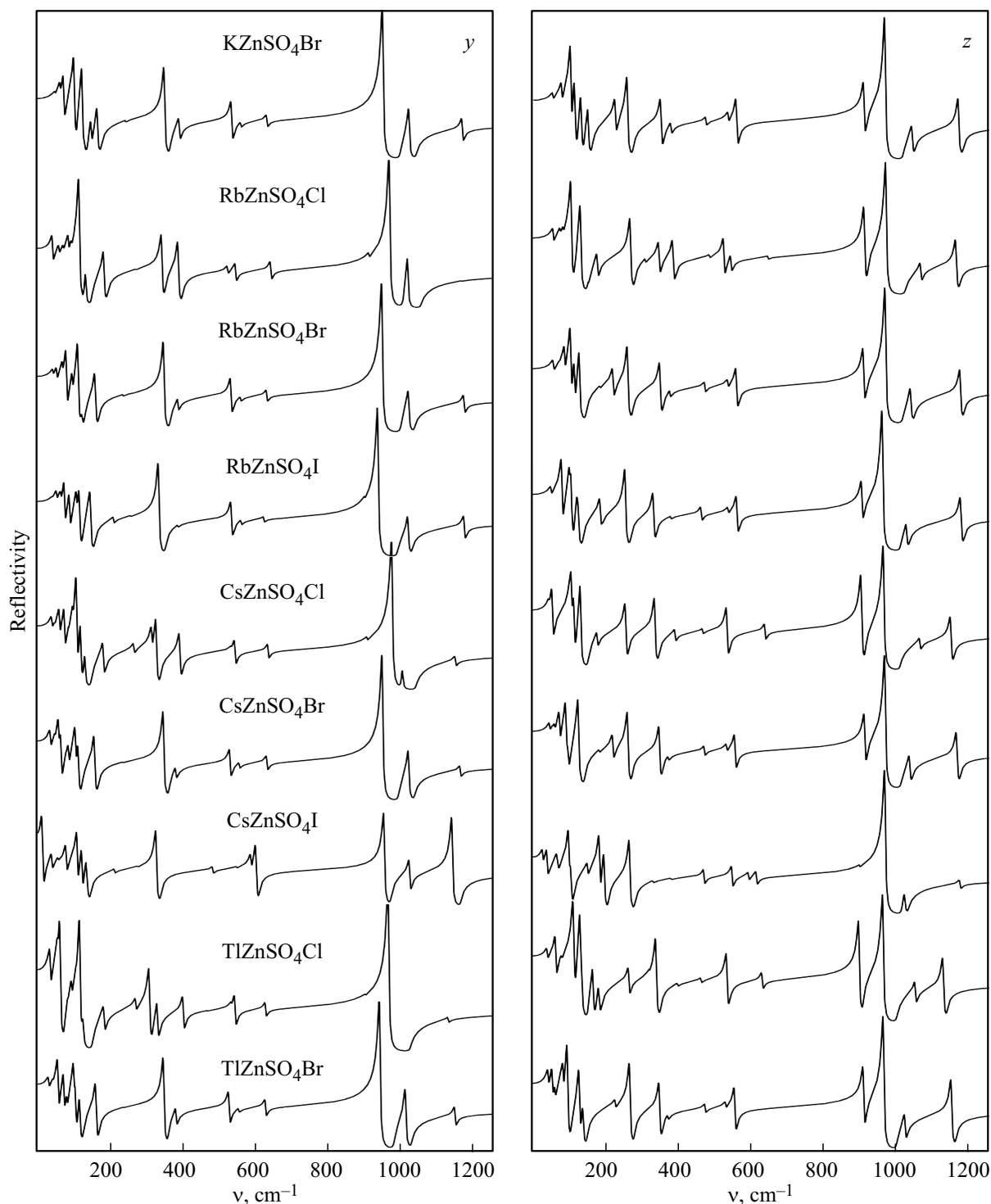


Figure 3. Reflection spectra of the belousovite type crystals with the $\mathbf{E} \parallel \mathbf{y}$ (left) and $\mathbf{E} \parallel \mathbf{z}$ (right) polarizations.

substances. Active RS modes of the $AZnSO_4X$ crystals with symmetry $P2_1/c$ are assigned to symmetry A_g and B_g . Intensity tensor for single-crystals with A_g has non-zero xx, xz, yy, zz components, while B_g has xy and yz . Intensity for the A_g -modes is usually higher than for B_g .

RS examinations have been previously conducted in the $ZnSO_4$ water solution [48], where four bands ν_3 in the

range of $1138\text{--}1056\text{ cm}^{-1}$, three bands ν_1 in the range of $854.5\text{--}992.5\text{ cm}^{-1}$, band ν_4 at 625 cm^{-1} and band ν_2 at 506 and 423 cm^{-1} were identified. The crystalline K_2SO_4 , Rb_2SO_4 , Cs_2SO_4 were investigated in detail in [50]. For A_g modes at 78 K in K_2SO_4 , ν_3 1152 and 1092 cm^{-1} , ν_1 989 cm^{-1} , ν_4 630 and 617 cm^{-1} and ν_2 450 cm^{-1} were measured. In the RS spectrum for Rb_2SO_4 , an intense band

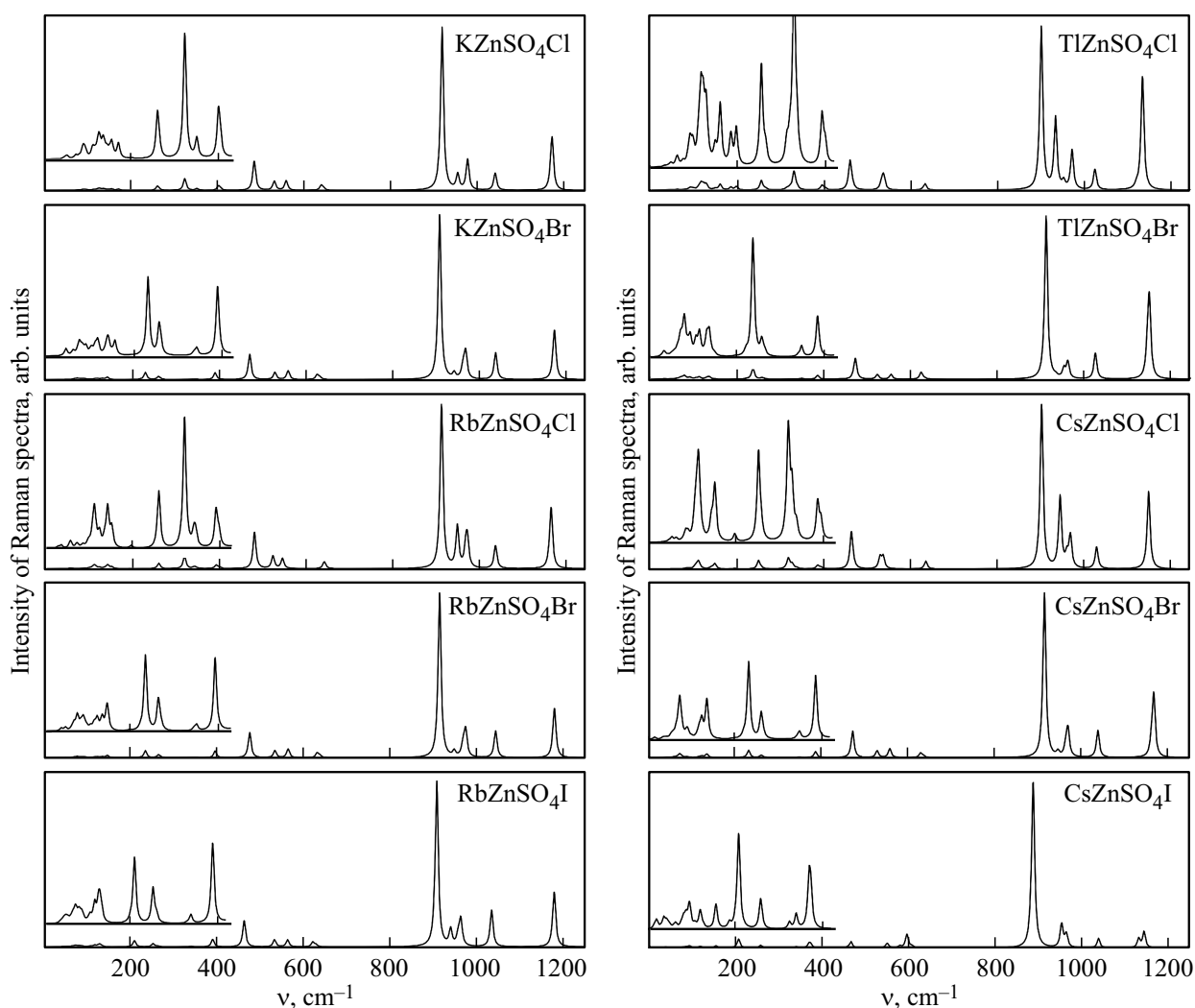


Figure 4. RS spectra of belousovite type crystals.

ν_1 at 980 cm^{-1} also prevails, and in Cs_2SO_4 , bands ν_1 – ν_4 are within 442 – 1119 cm^{-1} . Other measurements [12] show similar results.

The RS spectra of KZSC have a peak at 919 cm^{-1} formed by breathing A_g -modes of O atoms along the S-O bond lines. Its intensity is taken as 100%. Modes with an intensity of 10% at 955 and 978 cm^{-1} and a B_g mode at 978 cm^{-1} are also assigned to the same type (Figure 4). Together they form a ν_1 vibration group. As for the IR spectra, contribution of the O atoms is different. For the most intense spectrum, these are mainly O2 and O1 with 43% and 25%, respectively. Contributions to other vibrations are also made by the S atoms ($\sim 25\%$) and other O atoms, including O3 with a contribution of more than 60%. Group ν_3 is formed by the intense (31%) vibration with a wave number of 1174 cm^{-1} and two other B_g vibrations at 1042 and 1171 cm^{-1} . The first vibration is formed by the atomic displacements of O4 (66%) and S (27%) and the second one is formed by S and O1 (47%), O2 (16%). Deformation vibration region ν_2 is represented by two low-intensity

vibrations with wave numbers of 639 , 644 cm^{-1} formed primarily by the O1-O3 atoms. Deformation vibrations ν_4 of sulfate ion have an intense vibration at 483 cm^{-1} where O2 with the 30% contribution is distinguished together with the 20% involvement of the O1, O3 and O4 atoms. For other vibration with a wave number of 529 cm^{-1} , the O1, and O2 atoms prevail with the 25% contribution.

Lattice vibrations, where a considerable role is played by metal and chlorine atoms, have low intensity, therefore they are shown in a separate inset in Figure 4. A A_g mode with a wave number of 322 cm^{-1} formed by 23% Zn and 72% C atomic vibrations is distinguished among them. Vibration with the same symmetry at 259 cm^{-1} corresponds to the atomic displacements of Zn and O4. Vibrational mode with a wave number of 133 cm^{-1} is formed by 15% of K, 27% of Zn, 16% of Cl and 24% of O4 atoms.

Table 5 shows wave numbers of active A_g and B_g vibrations in RS. For all compounds, the A_g mode at $\sim 910\text{ cm}^{-1}$ is the most intense. However, the spectrum structure at ν_3 differs primarily in the line intensities. This is due to the

Table 5. Wave numbers (cm^{-1}) of the intramolecular vibrational modes $\nu_1 - \nu_4$ with symmetry A_g and B_g in the RS spectra of belousovite type crystals

Crystal	ν_3		ν_1		ν_4	ν_2	
	A_g	B_g	A_g	B_g	A_g	A_g	B_g
KZnSO ₄ Cl	1174	1171, 1042	919, 955, 978	978	639	483, 529, 558	556
KZnSO ₄ Br	1177	1175, 1040	915, 949, 974	971	629	475, 533, 564	562
RbZnSO ₄ Cl	1170	1166, 1041	916, 953, 976	973	644	483, 525, 548	527
RbZnSO ₄ Br	1180	1177, 1043	913, 947, 974	968	629	473, 531, 563	561
RbZnSO ₄ I	1180	1177, 1035	908, 940, 964	958	620	461, 532, 562	561
CsZnSO ₄ Cl	1156	1146, 1036	908, 951, 975	967	640	468, 534, 541	535
CsZnSO ₄ Br	1169	1164, 1040	916, 947, 971	966	629	472, 528, 558	557
CsZnSO ₄ I	1137	1149, 1044	893, 958, 970	968	600	471, 555, 584	599
TlZnSO ₄ Cl	1139	1125, 1029	905, 938, 976	957	636	462, 535, 540	536
TlZnSO ₄ Br	1155	1151, 1030	916, 938, 966	957	626	474, 525, 557	556

change in the S-O and A-O distances. Thus, in RCZI, the Cs atom environment includes seven O atoms: two of each Oo4, O2, O3, and one O1, and iodine atoms are farther than S. Intensity of modes ν_3 here is not higher than 10% and they are formed by atomic vibrations of 27% of S, 66% of O4 for the wave numbers of 1149, 1137 cm^{-1} and 29% of O1, 40% of O2 for 1044 cm^{-1} . Two vibrations ν_1 with symmetry A_g at 970, 958 cm^{-1} are also formed by $\sim 25\%$ of the S atomic displacements, the first mode is formed by 60% of O2 atoms and the second one is formed by 54% of O1 atoms. The most intense mode at 893 cm^{-1} is formed by the O atomic vibrations with the highest contribution of O3 equal to 52%. Oxygen atoms make approximately the same contribution to the B_g vibration at 888 cm^{-1} . As opposed to CZSI, intensity of modes ν_3 in TZSB is much higher. As in the previous case, they are formed by S atoms - 27%, O4 atoms - 67% and O1 atoms (bottom) - 49%. O1 and O3 atoms prevail by 60% and 47%, respectively, in the vibrational modes ν_1 at 967 and 957 cm^{-1} . RSS structure in the region of ν_3 , ν_1 is qualitatively similar for all bromine-containing compounds.

Correlation between vibrational spectra and structural parameters

Intramolecular modes ν_1 , ν_3 are formed by atomic vibrations of S and O1-O4 that make different contributions. This is due to different, though small, RS-O-distances and SO₄ rotations with respect to cations A (K, Rb, Cs, Tl) leading to different anionic environment R_{A-O} . This suggests that a linear dependence will take place between the frequencies of some vibrational modes and distances R_{S-O} . It can be used to determine frequencies by the known interatomic distances and, vice versa, to determine distances by the known frequencies.

For vibrations ν_1 and ν_3 that are active in IR spectra, substantial intensity will be shown in ascending order by modes designated as $1\nu_{1Bu}$, $2\nu_{1Au}$, $2\nu_{1Bu}$ and $1\nu_{3Au}$,

$1\nu_{3Bu}$, $2\nu_{1Bu}$, $2\nu_{1Au}$. Thus, for ν_{1Au} , the following dependence of the calculated wave numbers on the calculated distances between the S and O3 atoms is established: $\nu_{1Au} = 4359 - 2226R_{S-O3}$ with a correlation coefficient of 0.92. For the experimental values of R_{S-O3} and theoretical frequencies, the correlation coefficient will be certainly lower. Here, ν_1 is measured in cm^{-1} , and the distance is measured in Å. Consequently, the first coefficient is given in cm^{-1} and the second one is given in $\text{cm}^{-1}/\text{Å}$. For example, $R_{S-O3} = 1.5217 \text{ Å}$ in CZSC (Table 1), then ν_1 will be 971 cm^{-1} . Accurate calculation gives 973 cm^{-1} . Inverse equation is written as $R_{S-O3} = 1.895 - 0.0004\nu_{1Au}$. For the mode $1\nu_{3Bu} = 5476 - 2900R_{S-O3}$ (0.91). The correlation coefficient is given in brackets here. For other modes ν_3 , the following dependences will be obtained $1\nu_{3Au} = 3402 - 1562R_{S-O2}$ (0.882), $2\nu_{3Bu} = 4929 - 2466R_{S-O2}$ (0.82), $2\nu_{3Au} = 7841 - 4542R_{S-O4}$ (0.87). Similar equations may be also derived for other modes and S-O distances, but with lower correlation coefficients. For example, for the most intense vibration $2\nu_{3Bu} = -7885 + 5938R_{S-O1}$ (0.77).

For the RS spectra, linear dependences between the wave numbers and interatomic distances S-O may be established. The following mode sequence is used: $1\nu_{1Ag}$, $2\nu_{1Ag}$, $3\nu_{1Ag}$, $1\nu_{1Bg}$ and $1\nu_{3Ag}$, $1\nu_{3Bg}$, $2\nu_{3Bg}$ as shown in Table 4. For the most intense vibration, the dependence has a low correlation coefficient of 0.64: $1\nu_{1Ag} = 3527 - 1777R_{S-O4}$ and for other $3\nu_{1Ag} = 2041 - 699R_{S-O3}$ (0.77). For ν_3 , the correlation coefficients will be higher: $\nu_{3Ag} = 8592 - 5046R_{S-O4}$ (0.89), $1\nu_{3Bg} = 8753 - 5158R_{S-O4}$ (0.86). Correlation $\nu_{4Ag} = 3621 - 1956R_{S-O3}$ (0.81) may be also established.

Vibrational mode wave numbers are known to depend on the atomic weights and radii of cations. Their values of M_{AX} , R_{AX} were calculated as an average for cation A and halogen X. For modes ν_1 and ν_3 that are active in RSS, such dependences have correlation coefficients higher than 0.55, and the highest

value was calculated for $\nu_{1Bg} = 982 - 0.17M_{AX}$ (0.83) and $3\nu_{1Ag} = 1027 - 31.5R_{AX}$ (0.73).

Conclusion

Ab-initio density functional theory calculations with the exchange-correlation functional PBE and dispersion correction D3 have been conducted for belousovite mineral and its synthetic analogs with formula $AZnSO_4X$ ($A = K, Rb, Cs, Tl$; $X = Cl, Br, I$) with symmetry $P2_1/c$, and it has been shown that the structural features of crystals are exhibited in dielectric properties, IR reflection spectra and RSS.

Diagonal components of the electronic static dielectric tensor satisfy the condition $\epsilon_{\infty,x} > \epsilon_{\infty,y}, \epsilon_{\infty,z}$ and decay in the halogen series $I > Br > Cl$ inversely to the band gap. Maximum values of $\epsilon_{\infty,x}$ fall on the compounds with thallium. Diagonal components of the ionic dielectric tensor are subject to $\epsilon_{0,z} > \epsilon_{0,y} > \epsilon_{0,x}$.

LO modes ν_3 at 1052 cm^{-1} and ν_1 at 1002 cm^{-1} that are highly intense in $KZnSO_4Cl$ have large TO–LO splitting of -32 and -41 cm^{-1} . For the ν_3 -mode, it has inverse values $11.5, 2.1, 0.0\text{ cm}^{-1}$ in $AZnSO_4Cl$ ($A = Rb, Cs, Tl$), and the maximum values for ν_1 — $86.6, 66.0, 60.7\text{ cm}^{-1}$. For other LO-modes, ν_2 – ν_4 TO–LO splitting is maximum -4 cm^{-1} , and for ν_1 — it is lower than -1 cm^{-1} .

In the region below 400 cm^{-1} for the xz -polarization, two modes with symmetry B_u and two modes in the y -polarization with symmetry A_u that are corresponded by the translational vibrations of the O atoms with different share. Atomic vibrations involving cation A are within the region below 150 cm^{-1} , and in $KZnSO_4Cl$, these will be modes with the wave numbers of $149, 138, 128$ and 109 cm^{-1} for the xz -polarization and $123, 108\text{ cm}^{-1}$ for the y -polarization. In other compounds, intensities of these lines differ substantially which is attributable to the participation of cations with different atomic weight.

In the RS spectrum, the intramolecular modes ν_1, ν_3 will be most intense. The first group contains three vibrations with symmetry A_g and one vibration with symmetry B_g , the most intense one from which (at 900 – 920 cm^{-1}) is induced to a greater extent by the O1 and O3 atoms, and the other three vibrations are induced by S and other O atoms. On the contrary, modes with the wave numbers higher than 1100 cm^{-1} have a prevailing contribution of the O4 atoms. Different involvement of non-equivalent O atoms is responsible for the differences in the spectra of compounds in this region. For sulfate ion vibrations ν_4, ν_2 four peaks are distinguished in the spectra, among which vibrations with wave numbers of 460 – 480 cm^{-1} have substantial intensity.

The vibrational mode wave numbers depend on inter-atomic distances, atomic weights and radii of cations A and anions X. Thus, for modes ν_3 , linear dependences of the wave numbers on the distances between the S and O4 atoms have been determined phenomenologically: $\nu_{3Ag} = 8592 - 5046R_{S-O4}$, $\nu_{3Bg} = 8753 - 5158R_{S-O4}$. For mode ν_1 , a linear dependence on the mean atomic weight

of cation A and anion X is shown: $\nu_{1Bg} = 982 - 0.17M_{AX}$. The derived equations may be used to predict the corresponding experimental dependences in compound identification and to determine frequencies by the known distances and distances by the known frequencies.

Conflict of interest

The author declares that he has no conflict of interest.

References

- [1] O.I. Siidra, E.V. Nazarchuk, E.A. Lukina, A.N. Zaitsev, V.V. Shilovskikh. *Mineral. Mag.*, **82**, 1079 (2018). DOI: 10.1180/minmag.2017.081.084
- [2] I.V. Pekov, A.A. Agakhanov, N.V. Zubkova, N.N. Koshlyakova, N.V. Shechipalkina, F.D. Sandalov, V.O. Yapaskurt, A.G. Turchkova, E.G. Sidorov. *Russian Geology and Geophysics.*, **61** (5–6), 675 (2020). DOI: 10.15372/RGG2019167.
- [3] A.S. Borisov, O.I. Siidra, D.O. Charkin, K.A. Zagidullin, R.K. Burshtynovich, N.S. Vlasenko. *Acta Crystallogr. B*, **78**, 499 (2022). DOI: 10.1107/S2052520622003535
- [4] B. Bosson. *Acta Crystallogr. B*, **32**, 2044 (1976).
- [5] A. Oganov. *Faraday Discuss.*, **211**, 643 (2018). DOI: 10.1039/C8FD90033G
- [6] C. Richard, A. Catlow. *IUCr J.*, **10** (2), 143 (2023). DOI: 10.1107/S2052252523001835
- [7] S.A. Klimin, B.N. Mavrin, I.V. Budkin, V.V. Badikov, D.V. Badikov. *Opt. Spectrosc.*, **127** (1), 14 (2019). DOI: 10.1134/S0030400X19070130.
- [8] V.A. Chernyshev, P.A. Agzamova, A.V. Arkhipov. *Opt. Spectrosc.*, **128** (11), 1800 (2020). DOI: 10.1134/S0030400X20110090.
- [9] Yu.N. Zhuravlev, *Opt. i spektr.*, **131** (9), 1199 (2023) (in Russian). DOI: 10.61011/OS.2023.09.56606.4667-23
- [10] J.J. Wylde, G.C. Allen, I.R. Collins. *Appl. Spectrosc.*, **55**, 1155 (2001). <https://opg.optica.org/as/abstract.cfm?URI=as-55-9-1155>
- [11] H. Takahashi, S. Meshitsuka, K. Higasi. *Spectrochim. Acta A: Molec. Spectrosc.*, **31** (11), 1617 (1975). DOI: 10.1016/0584-8539(75)80102-4
- [12] K. Ben Mabrouk, T.H. Kauffmann, H. Aroui, M.D. Fontana. *J. Raman Spectrosc.*, **44** (11), 1603 (2013). DOI: 10.1002/jrs.4374ff
- [13] J. Qiu, X. Li, X. Qi. *IEEE Photonics J.*, **11** (5), 6802612 (2019). DOI: 10.1109/JPHOT.2019.2939222
- [14] A.R. Aliev, I.R. Akhmedov, M.G. Kakagasanov, Z.A. Aliev. *Phys. Solid State*, **61** (8), 1464 (2019). DOI: 10.1134/S1063783419080043.
- [15] D.V. Korabel'nikov, Yu.N. Zhuravlev. *J. Phys. Chem. Solids*, **119**, 114 (2018). DOI: 10.1016/j.jpcs.2018.03.037
- [16] K. Omori. *Mineral. J.*, **5** (5), 334 (1968).
- [17] M.D. Lane. *American Mineralogist*, **92** (1), 1 (2007). DOI: 10.2138/am.2007.2170
- [18] R. Dovesi, A. Erba, R. Orlando, C.M. Zicovich-Wilson, B. Civalleri, L. Maschio, M. Rérat, S. Casassa, J. Baima, S. Salustro, B. Kirtman. *WIREs Comput. Mol. Sci.*, **8** (4), e1360 (2018). DOI: 10.1002/wcms.1360
- [19] L. Valenzano, F.J. Torres, K. Doll, F. Pascale, C.M. Zicovich-Wilson, R. Dovesi. *Zeitschrift für Physikalische Chemie*, **220** (7), 893 (2006). DOI: 10.1524/zpch.2006.220.7.893

- [20] T. Bredow, P. Heitjans, M. Wilkening. *Phys. Rev. B*, **70** (11), 115111 (2004). DOI: 10.1103/PhysRevB.70.115111
- [21] J.E. Jaffe, A.C. Hess. *Phys. Rev. B*, **48** (11), 7903 (1993). DOI: 10.1103/PhysRevB.48.7903
- [22] E. Apra, M. Causa, M. Prencipe, R. Dovesi, V.R. Saunders. *J. Phys. Condens. Matter*, **5** (18), 2969 (1993). DOI: 10.1088/0953-8984/5/18/019
- [23] K. Doll, H. Stoll. *Phys. Rev. B*, **57** (8), 4327 (1998). DOI: 10.1103/PhysRevB.57.4327
- [24] J. Laun, D.V. Oliveira, T. Bredow. *J. Comput. Chem.*, **39** (19), 1285 (2018). DOI: 10.1002/jcc.25195
- [25] J. Laun, T. Bredow. *J. Comput. Chem.*, **42** (15), 1064 (2021). DOI: 10.1002/jcc.26521
- [26] J.P. Perdew, K. Burke, M. Ernzerhof. *Phys. Rev. Lett.*, **77**, 3865 (1996). DOI: 10.1103/PhysRevLett.77.3865
- [27] S. Grimme, S. Ehrlich, L. Goerigk. *Comput. Chem.*, **32** (7), 1456 (2011). DOI: 10.1002/jcc.21759
- [28] E.M. Roginskii, Y.F. Markov, A.I. Lebedev. *J. Experiment. Theor. Phys.*, **128** (5), 727 (2019). DOI: 10.1134/S1063776119030208.
- [29] R. Dovesi, V.R. Saunders, C. Roetti, R. Orlando, C.M. Zicovich-Wilson, F. Pascale, B. Civalleri, K. Doll, N.M. Harrison, I.J. Bush, P. D'Arco, M. Llunell, M. Causà, Y. Noël, L. Maschio, A. Erba, M. Rerat, S. Casassa. *CRYSTAL17 User's Manual* (University of Torino, Torino, 2017).
- [30] H.J. Monkhorst, J.D. Pack. *Phys. Rev. B*, **13** (11), 5188 (1976). DOI: 10.1103/PhysRevB.13.5188
- [31] C.G. Broyden. *IMA J. Appl. Math.*, **6**, 76 (1970).
- [32] R. Fletcher. *Comput. J.*, **13**, 317 (1970).
- [33] D. Goldfarb. *Math. Comput.*, **24**, 23 (1970).
- [34] F. Shanno. *Math. Comput.*, **24**, 647 (1970).
- [35] F. Pascale, C.M. Zicovich-Wilson, F. Lopez, B. Civalleri, R. Orlando, R. Dovesi. *J. Comput. Chem.*, **25** (6) 888 (2004). DOI: 10.1002/jcc.20019
- [36] C.M. Zicovich-Wilson, F. Pascale, C. Roetti, V.R. Saunders, R. Orlando, R. Dovesi. *J. Comput. Chem.*, **25** (15), 1873 (2004). DOI: 10.1002/jcc.20120
- [37] P. Umari, A. Pasquarello, A. Dal Corso. *Phys. Rev. B*, **63** (9), 094305 (2001). DOI: 10.1103/PhysRevB.63.094305
- [38] X. Gonze, C. Lee. *Phys. Rev. B*, **55** (16), 10355 (1997). DOI: 10.1103/PhysRevB.55.10355
- [39] R. Resta. *Rev. Mod. Phys.*, **66** (3), 899 (1994). DOI: 10.1103/RevModPhys.66.899
- [40] C. Carteret, M. De La Pierre, M. Dossot, F. Pascale, A. Erba, R. Dovesi. *J. Chem. Phys.*, **138**, 014201 (2013). DOI: 10.1063/1.4772960
- [41] M. Ferrero, M. Rerat, R. Orlando, R. Dovesi. *J. Chem. Phys.*, **128**, 014110 (2008). DOI: 10.1063/1.2817596
- [42] A. Erba, R. Dovesi. *Phys. Rev. B*, **88** (4), 045121 (2013). DOI: 10.1103/PhysRevB.88.045121
- [43] L. Maschio, B. Kirtman, M. Rerat, R. Orlando, R. Dovesi. *J. Chem. Phys.*, **139**, 164102 (2013). DOI: 10.1063/1.4824443
- [44] R.D. Shannon. *Acta Cryst. A*, **32**, 751 (1976).
- [45] V.M. Fridkin, T.G. Golovina, A.F. Konstantinova, E.A. Evdshchenko. *Crystallography Reports*, **67** (4), 494 (2022). DOI: 10.1134/s1063774522040083.
- [46] I. Petousis, D. Mrdjenovich, E. Ballouz, M. Liu, D. Winston, W. Chen, T. Graf, T.D. Schladt, K. Persson, F.B. Prinz. *Sci. Data*, **4**, 160134 (2017). DOI: 10.1038/sdata.2016.134
- [47] R. Demichelis, H. Suto, Y. Noel, H. Sogawa, T. Naoi, C. Koike, H. Chihara, N. Shimobayashi, M. Ferrabone, R. Dovesi. *Mon. Not. R. Astron. Soc.*, **420**, 147 (2012). DOI: 10.1111/j.1365-2966.2011.20018.x
- [48] W.W. Rudolph, M.H. Brooker, P.R. Tremaine. *J. Solution Chem.*, **28** (5), 621 (1999). DOI: 10.1023/A:1022691117630
- [49] V. Karadjova, D. Stoilova. *J. Crystall. Process and Technology*, **3**, 136 (2013). DOI: 10.4236/jcpt.2013.34022
- [50] D. Liu, H.M. Lu, J.R. Hardy, F.G. Ullman. *Phys. Rev. B.*, **44** (14), 7387 (1991). DOI: 10.1103/PhysRevB.44.7387

Translated by E.Ilinckaya